ORIGINAL ARTICLE

Tensile fatigue behaviour of ultra-high performance fibre reinforced concrete (UHPFRC)

Tohru Makita · Eugen Brühwiler

Abstract The tensile fatigue behaviour of ultra-high performance fibre reinforced concrete (UHPFRC) under constant amplitude fatigue cycles is presented. Three series of uniaxial tensile fatigue tests up to a maximum of 10 million cycles were conducted with the objective to determine the endurance limit of UHPFRC that was supposed to exist for this material. The fatigue tests reveal that an endurance limit exists in all three domains of UHPFRC tensile behaviour at S-ratios ranging from 0.70 to 0.45 with S being the ratio of the maximum fatigue stress to the elastic limit strength of UHPFRC. Rather large variation in local specimen deformations indicates significant stress and deformation redistribution capacity of the UHPFRC bulk material enhancing the fatigue behaviour. The fatigue fracture surface of UHPFRC shows features of the fatigue fracture surfaces of steel, i.e. fatigue crack propagation is identified by a smooth surface while final fracture leads to rather rough surface. Various fatigue damaging mechanisms due to fretting and grinding as well as tribocorrosion are identified.

T. Makita (✉) · E. Brühwiler
Laboratory of Maintenance and Safety of Structures (MCS), Ecole Polytechnique Fédérale de Lausanne (EPFL), Station 18, 1015 Lausanne, Switzerland
e-mail: tohru.makita@epfl.ch
URL: http://mcs.epfl.ch/

E. Brühwiler
e-mail: eugen.bruehwiler@epfl.ch

1 Introduction

Due to ever increasing traffic demands, deck slabs of bridges are subjected to significant fatigue loading. A novel method of rehabilitation and strengthening of bridge deck slabs in reinforced concrete (RC) is the casting of a 30–50 mm layer of ultra-high performance fibre reinforced concrete (UHPFRC) with or without steel rebars on top of the existing slab. This method has proven to be technically more efficient and more economic than conventional methods consisting of adding an additional RC layer on the deck slab [1–4]. In order to validate this concept, the fatigue behaviour of UHPFRC needs to be known and the fatigue strength determined.

UHPFRC is a cementitious fibre reinforced composite material showing eminent mechanical properties such as relatively high strength, i.e., tensile strength higher than 10 MPa with significant deformation capacity, compressive strength higher than 180 MPa and low-permeability providing very high resistance against penetration of water and other substances, thus enhancing durability.

A typical stress–strain response of UHPFRC from a quasi-static tensile test shows the following three domains (Fig. 1):

– The *elastic domain* is governed by the behaviour of the matrix until it reaches its tensile strength, called the elastic limit strength. Microcracks start to form at the stress level in the vicinity of the elastic limit.

– These microcracks are bridged and controlled by fibres. After entering the *strain-hardening domain* more microcracks develop in the whole specimen volume. A considerable reduction in modulus of deformation, i.e. the ratio of stress to strain, is observed. The strain-hardening extends until the ultimate resistance or tensile strength is reached in the weakest section of the specimen.

– In the *strain-softening domain* beyond ultimate strength, a discrete macrocrack forms in this weakest section and becomes eventually visible. Consequently, deformation localizes in the macrocrack zone while the zones outside are unloading. Finally the specimen fractures into two parts at the end of softening.

In this paper, a microcrack is defined as a crack not visible to the naked eye and its width is smaller than 0.05 mm. A macrocrack is defined as a crack visible to the naked eye and its width is larger than 0.05 mm; it occurs only in the post-peak softening domain.

The objective of this paper is to describe the tensile fatigue behaviour of UHPFRC. Despite a more demanding test set-up, uniaxial tensile fatigue tests (rather than bending tests) were conducted on monolithic UHPFRC plates thus providing more objective results. The experimental campaign is described and the test results are analysed and interpreted.
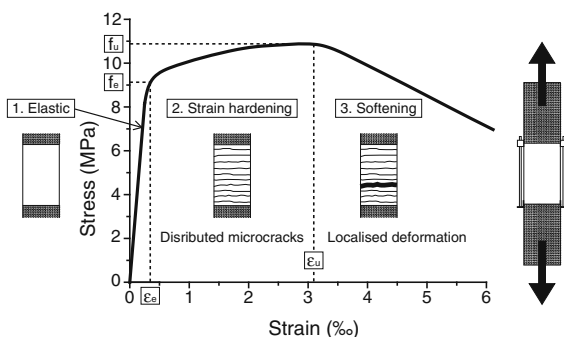

Fig. 1 Schematic representation of tensile response of UHPFRC

2 Literature review

Four-point bending fatigue tests were carried out on specimens made of CERACEM®, a commercial UHPFRC [5]. A linear relation was found between the number of cycles and the deflection growth rate in the stage where deflection constantly increased. An endurance limit at 10 million cycles could however not be determined due to the large scatter of test results which was attributed to strength variations within the specimens.

Behloul et al. [6] performed three-point bending fatigue tests on Ductal® using steel fibres. Specimens were first subjected to quasi-static flexural force preceding bending fatigue tests until the strain in the extreme tension fibre at the mid-span of specimens reached 0.30 ‰. Only one combination of fatigue minimum and maximum force, i.e. 10 and 90 % of the bending elastic limit strength was applied under force control. Fatigue testing was stopped after about 1 million cycles where only little damage was observed on all specimens. After fatigue testing, the specimens were subjected to quasi-static flexural force again and there was no influence of preceding bending fatigue loading on the ultimate resistance of the specimens. An endurance limit at 1 million cycles was estimated to be at about 54 % of the elastic limit strength.

Farhat et al. [7] conducted force-controlled three-point bending fatigue tests on high performance fibre reinforced cementitious composites (HPFRCCs) named CARDIFRC® using specimens of two sizes. Scatter was observed in the results from larger specimens. Consistent results were obtained from the smaller specimens. The endurance limit at 1 million cycles was evaluated to be at 85 % of the flexural strength of the specimens. No visible cracks were observed on the fatigue tested smaller specimens that sustained 1 million cycles. The fracture surfaces of larger specimens revealed areas devoid of fibres in the fracture surface, especially in the tensile zone or had many but poorly orientated fibres. Moreover, image analysis showed that the fracture surface had less homogenous and less dense fibre distribution when compared to other sections of the specimen.

Parant et al. [8] carried out four-point bending fatigue tests on UHPFRC of the $CEMTEC^{®}_{multiscale}$ type including three different types of fibres. The endurance limit was evaluated as 65 % of bending tensile stress for 2 million cycles.

Fitik et al. [9, 10] performed uniaxial stress reversal and tensile fatigue tests on ultra high performance concrete (UHPC) using four different mixes. The scatter in test results was attributed to local defects initiating and accelerating failure progression. Deformation growth during the fatigue tests was demonstrated to be divided into three stages similar to concrete, namely rapid deformation growth due to initial crack formation in the first stage, stable deformation growth with constant crack propagation rate in the second stage and rapid deformation growth to failure caused by instable crack growth.

This literature review reveals that comprehensive uniaxial tensile fatigue testing of UHPFRC has not been performed so far and knowledge of tensile fatigue behaviour of UHPFRC is rather scarce. In previous studies, bending fatigue tests were often conducted because of experimental simplicity and the number of cycles was often limited to 1 million. One may question whether bending fatigue tests provide objective results as stress redistribution occurs in bent sections [11].

3 Experimental campaigns

3.1 Specimens, test set-up and instrumentation

The in-house developed UHPFRC mix called HIF-COM 13 was used for the experiments. This mix is characterised by 3.0 vol.% content of 13 mm long steel fibres with a diameter of 0.16 mm and by the use of CEM III/B type cement which contains a high percentage of blast furnace slag (66–80 %) (Table 1).

The chosen specimen is 750 mm long with a cross section of 150×40 mm^2 (Fig. 2). Specimens were cast in wooden forms and demoulded 7 days after casting, and then kept in the testing hall at constant climate condition. In order to cause fracture within the 250 mm-long central zone of the specimen, aluminium plates (250 mm long, 150 mm wide and 2 mm thick) were glued using epoxy resin to both surfaces of the specimen end parts as strengthening elements.

Two 250 mm-long linear variable differential transducers (LVDTs) and five displacement transducers with a 50 mm measurement length were used to measure the specimen deformation (Fig. 2). LVDTs were set up on both of specimen sides such as to capture global specimen deformation. In this paper the average of deformation as measured by the two LVDTs are always referred to as global deformation. The five displacement transducers were set up on the specimen surface to measure local specimen deformation in five consecutive zones. Force was measured by the load cell installed in the actuator of the 1,000 kN servo-hydraulic testing machine.

Deformation and force data were recorded with a frequency of 200 Hz. The initial and final phases of the test were recorded permanently, while between these phases data was recorded for 1 s every 600 cycles.

All specimens were cast on the same day. They had an age of more than 56 days when tested.

3.2 Determination of elastic limit strength

Three quasi-static tensile tests were conducted per test parameter to determine the quasi-static specimen behaviour as well as the elastic limit and ultimate strengths. Ultimate strength is defined as the maximum force UHPFRC was resisting during the test divided by the nominal cross section area. The elastic limit strength cannot always be identified clearly by a distinct point on the stress–strain curve. Adopting methods to determine modulus of elasticity of concrete and yield strength of steels, a method to determine the elastic limit strength of UHPFRC was developed as shown in Fig. 3:

- Firstly, point P1 is chosen at 3 MPa assuming that this lower stress level is at about 30 % of the expected elastic limit strength (of about 10 MPa) such as to eliminate initial nonlinear stress carrying effects often observed for cementitious materials; point P2 at 6 MPa is chosen as an upper stress level of about 60 % of the expected elastic limit strength.
- A line L1 passing through P1 and P2 is drawn to find P3 as the intersection with the strain axis.
- Line L1 is then translated by 0.1 ‰ to obtain the parallel line L2 which intersects with the recorded stress–strain curve to finally define the elastic limit strength (point P5) and the corresponding elastic limit strain.
- Moreover, the modulus of elasticity of UHPFRC E_U is determined as the slope of line L.

Using this method, average elastic limit strength and strain of the investigated UHPFRC was determined to be 8.2 MPa and 0.32 ‰ respectively.

Table 1 Composition of UHPFRC (HIFCOM 13)

Component	Type	Mass (kg/m^3)	Remarks
Cement	CEM III/B	1277.4	
Silica fume	Elkem Microsilica 971 U	95.8	7.5 % of cement mass
Sand	Quartz sand MN 30	664.6	$d_{max} < 0.5$ mm
Steel fibres	Bekaert OL 13/0.16 mm	235.5	3.0 vol.%, brass coating
Superplasticiser	Sikament P5	42.3	3.3 % of cement mass
Water		198.0	W/C = 0.155

3.3 Testing program

3.3.1 Objectives

Three series of constant amplitude tensile fatigue tests were conducted at various imposed fatigue stress levels as characterized by varying maximum stress and pre-applied deformation. Each fatigue test series is characterised referring to the quasi-static stress–strain curve following (Fig. 4):

– *S1 series* maximum stress high in the elastic domain
– *S2 series* initial application of deformation entering into the strain-hardening domain followed by fatigue testing
– *S3 series* initial application of deformation entering into the softening domain followed by fatigue testing

The objective of the S1 series was the determination of the endurance limit within the elastic domain. The comprehension of tensile fatigue behaviour beyond the elastic limit after losing the initial modulus of deformation of the specimen was the objective for the S2 and S3 series.

In this paper, the endurance limit is defined as a stress level below which no fatigue failure occurs up to
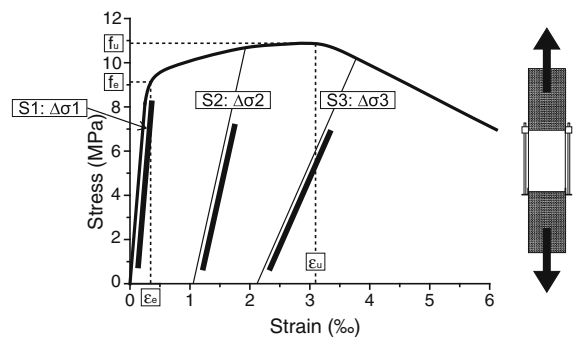

Fig. 2 Specimen geometry, measuring devices and testing set-up

Fig. 3 Determination of elastic limit strength of UHPFRC

Fig. 4 Schematic representation of tensile response of UHPFRC and definition of tensile fatigue test series

10 million cycles. With respect to bridge deck slabs, 10 million extreme stress cycles are considered to be realistic for heavily trafficked bridges. Also, limited available time for the experimental campaign imposed a maximum number of 10 million cycles which is usually considered as a lower bound of the very high cycle fatigue domain [12].

3.3.2 S1 series: tensile fatigue behaviour within the elastic domain

In preliminary fatigue tests, a specimen sustained 10 million cycles at a maximum stress of 7.2 MPa (and minimum stress of 0.82 MPa), then a second time 10 million cycles after increasing to 8.5 MPa maximum tensile stress and failed (fractured) finally after 7.45 million cycles at a maximum tensile fatigue stress of 10 MPa.

From this preliminary test result the endurance limit of the investigated UHPFRC was supposed to exist between 8.5 and 10 MPa which is in the domain of the elastic limit strength. To verify this supposition, S1 series were conducted to have maximum stress at high stress levels within the elastic domain.

Maximum stress was determined by the following procedure: first, the specimen was subjected to quasi-static tensile stress until one LVDT reached a target deformation (corresponding to strains of either 0.20, 0.25 or 0.30 ‰) and unloaded. The stress that caused the target deformation was then applied as maximum stress level for the fatigue test. Because of the variation of elastic limit strength (which is most likely due to local variations of fibre distribution and orientation [13]), deformation (instead of stress) provides more reliable information about the tensile behaviour of UHPFRC.

Three target strain values were chosen assuming that if the strain caused by the initial cycle is smaller than 0.25 ‰, UHPFRC under the corresponding tensile fatigue stress can sustain 10 million cycles. This threshold strain value of 0.25 ‰ was justified from results of the preliminary tensile fatigue test. The idea of a threshold strain value for the endurance limit was also taken from findings of Parant et al. [8].

The minimum fatigue stress was always set equal to 10 % of the average elastic limit strength as determined from three quasi-static tensile tests. In the real structural member, complete unloading is unlikely to occur. Therefore, small stress was given as a minimum fatigue stress. 10 % of the average elastic limit strength was arbitrarily chosen.

3.3.3 S2 and S3 series: fatigue behaviour after preloading into the strain-hardening and softening domains

When a UHPFRC layer is cast on an existing concrete element, tensile eigenstresses develop in the UHPFRC due to restrained shrinkage. The combination of these eigenstresses and stresses due to external action effects, i.e. due to permanent and traffic loads in the case of bridge deck slab, may result in tensile stress in the UHPFRC entering into the strain-hardening domain. Subsequently, initial deformation modulus is significantly reduced preventing further stress increase in the UHPFRC layer [14]. S2 and S3 series were designed to reproduce such situations. For this, deformation corresponding to strains of between 0.5 and 4 ‰ in S2 series and to strains of between 3 and 6 ‰ for S3 series was imposed prior to starting the fatigue test.

Maximum fatigue stress was applied using again the method for S1 series considering the stress–strain curve obtained from the initially imposed quasi-static tensile deformation. The stress causing a specific global deformation was imposed as maximum fatigue stress, i.e. the stress corresponding to strains of either 0.10, 0.15 or 0.20 ‰. The minimum fatigue stress was always 10 % of maximum stress in both S2 and S3 series.

3.3.4 Testing procedure

All quasi-static tensile tests were conducted in a displacement-controlled mode with a displacement rate of 0.02 mm/min.

The fatigue stress application procedure was as follows. Firstly, stress was increased to the specified maximum stress under displacement control mode with a rate of 0.02 mm/min, then sinusoidal wave cyclic stress was imposed under force control mode with a frequency of 10 Hz. 10 s were needed for the transition period from quasi-static to the constant amplitude cyclic stress regime.

When a specimen sustained 10 million cycles, this result was regarded as 'run-out', and the test subsequently was continued at an increased maximum tensile fatigue stress.

4 Results and discussion of experimental tests

4.1 Fatigue strength and endurance limit

4.1.1 Overview of results

Table 2 summarises the results of tensile fatigue tests on UHPFRC specimens. Specimens were regarded as failed when the average of two global deformation readings reached 2.5 mm, corresponding to 10 ‰ of strain.

Due to logistic reasons, S1-1_i and S2-4_i test had to be stopped at 5 million cycles, and S2-4_ii test at 2 million cycles. S1-3_i test was continued until 20 million cycles in order to observe how the behaviour of UHPFRC changes when it is subjected to the fatigue cycles twice as high as the specified one, i.e. 10 million cycles. As a result, no obvious change was observed in the fatigue behaviour of UHPFRC.

An S–N diagram (Wöhler diagram) is adequate to represent results from fatigue tests and to determine the fatigue resistance. For cementitious materials, the ratio of maximum applied fatigue stress to tensile strength is often used as fatigue stress indicator S, in order to eliminate variations in material composition, specimen size and testing setup. A log scale is commonly used for the number of stress cycles N.

Figure 5 shows the S–N diagrams as obtained in the present study for UHPFRC, where S is determined as the ratio of maximum fatigue stress to the elastic limit strength f_e.

– In the case of the S1 series, the elastic limit strength obviously could not be determined for each specimen, and the average value of elastic limit strength as obtained from three quasi-static tensile tests was used to calculate S.
– As the specimens of S2 and S3 series were subjected to preloading beyond the elastic limit strength before fatigue testing, the value of elastic limit strength $f_{e,i}$ could be determined for each specimen.

4.1.2 Test series S1

Rather large scatter is observed on the S–N diagram (Fig. 5a) which may be due to elastic limit strength value used to calculate the fatigue stress indicator S. Obviously, this elastic limit strength value is either too high or too low for single specimens in comparison

with their own specific elastic limit strength. Consequently, S values of some tests are quite higher or lower than 1 despite the fact that the applied maximum fatigue stress was always smaller than the elastic limit strength.

Nevertheless, the results may be used to estimate the endurance limit of the S1 series. From the overall test results including all run-outs, the endurance limit may be estimated to be around $S = 0.70$ (as indicated by the horizontal dashed lines in Fig. 5a). At maximum fatigue stress levels above the endurance limit, the results indicate rather short fatigue lives confirming the hypothesis that UHPFRC under fatigue tensile stress above a certain limit, i.e. the endurance limit, shows only small fatigue resistance.

4.1.3 Test series S2

The results shown in Fig. 5b indicate a fatigue strength that may be expressed by a linear relation between $\sigma_{max}/f_{e,i}$ and $\text{Log} N$. A linear regression line was determined (without considering run-outs) with a correlation coefficient of 0.69, indicating reasonably good dependency between the two variables:

$$\frac{\sigma_{max}}{f_{e,i}} = -0.105 \cdot \log N + 1.436 \tag{1}$$

The test results including the run-outs again allow estimating the endurance limit to be at an S-level of about 0.55–0.65 (as indicated by the horizontal dashed lines in Fig. 5b).

4.1.4 Test series S3

Only few results are available (Fig. 5c) and a relation describing the fatigue strength cannot be determined. The endurance limit may be estimated to be at about $S = 0.45$ (as indicated by a dashed horizontal line in Fig. 5c).

Moreover, the magnitude of pre-applied deformation seems to have a major influence on the fatigue behaviour. Specimen S4-5 (not shown on Fig. 5c) was subjected during preloading to a relatively high deformation into softening domain of 6 ‰ which was significantly higher than for the other specimens. Due to this preloading, a significant damage was probably induced in the specimen and subsequently, only relatively short fatigue life resulted. This indicates low fatigue strength for high deformation into

Table 2 Results of tensile fatigue tests of UHPFRC

Test No.	Stress		Sustained cycles	Remarks
	σ_{max} (MPa)	σ_{min} (MPa)		
Preliminary test				
1				
i	7.2	0.82	10.00×10^6	Run-out
ii	8.5	0.82	10.00×10^6	Run-out
iii	10.0	0.82	7.45×10^6	
S1 series				
1				
i	5.0	0.82	5.00×10^6	Run-out
ii	6.6	0.82	0.35×10^6	
2	6.1	0.00	0.29×10^6	
3				
i	7.8	0.82	20.00×10^6	Run-out
ii	8.7	0.82	0.43×10^6	
4	8.1	0.82	0.28×10^6	
5				
i	8.2	0.82	10.00×10^6	Run-out
ii	10.8	0.82	61,108	
6	8.2	0.82	0.29×10^6	
7	8.5	0.82	0.15×10^6	
8	9.4	0.82	0.16×10^6	

Test No.	Stress		Sustained cycles	Elastic limit strength (MPa)	Pre-applied strain (‰)	Remarks
	σ_{max} (MPa)	σ_{min} (MPa)				
S2 series						
1	7.4	0.74	7.78×10^6	10.9	0.48	
2						
i	6.3	0.63	10.07×10^6	10.1	0.50	Run-out
ii	7.8	0.78	10.06×10^6			Run-out
iii	8.8	0.88	7.09×10^6			
3						
i	5.9	0.59	10.00×10^6	10.5	1.13	Run-out
ii	8.4	0.84	3.11×10^6			
4						
i	6.9	0.69	5.00×10^6	10.7	1.99	Run-out
ii	9.0	0.90	2.00×10^6			Run-out
iii	10.4	1.04	64,717			
5						
i	7.6	0.76	10.00×10^6	12.5	2.01	Run-out
ii	11.7	1.17	0.11×10^6			
6	5.2	0.52	7.87×10^6	9.0	2.09	
7						
i	6.7	0.67	10.08×10^6	10.3	3.00	Run-out
ii	8.7	0.87	84,075			

Table 2 continued

Test No.	Stress		Sustained cycles	Elastic limit strength (MPa)	Pre-applied strain (‰)	Remarks
	σ_{max} (MPa)	σ_{min} (MPa)				
8						
i	6.0	0.60	11.36×10^6	10.3	4.00	Run-out
ii	7.9	0.79	1.60×10^6			
S3 series						
1						
i	6.0	0.60	10.00×10^6	10.0	3.02	Run-out
ii	7.2	0.72	10.02×10^6			Run-out
iii	8.3	0.83	3.01×10^6			
2	5.3	0.53	9.20×10^6	11.5	4.00	
3						
i	4.9	0.49	10.00×10^6	10.7	5.01	Run-out
ii	6.7	0.67	2.61×10^6			
4						
i	4.5	0.45	10.00×10^6	8.4	5.03	Run-out
ii	6.6	0.66	14,146			
5	4.4	0.44	25,228	8.8	6.11	

the softening domain. This may be explained by significant fibre pull-out due to such large deformations.

4.2 Deformation behaviour

In the present study, uniaxial tensile force was applied to specimens in both quasi-static and fatigue tests. Given the constant specimen cross section, nominal tensile stress in UHPFRC is equal in any cross section. Yet, local deformation as measured with the five displacement transducers varied significantly over the specimen length as discussed in the following based on experimental observations.

Figure 6a shows stress-local deformation curves as obtained from quasi-static tensile preloading of S4-1 fatigue test, and Fig. 6b is a magnified view of the stress-local deformation relationship. Loading was stopped when the global strain reached 3 ‰ (Fig. 6c).

In the initial phase, deformation of all zones G1 to G5 increased similarly until stress reached about 4.5 MPa from where on significantly larger deformation readings were recorded in the G4 zone which entered first into the hardening domain. At 5 MPa, deformation readings increased significantly also in G5, followed by G1 and G3 zones at about 8 MPa and

finally G2 zone at about 13 MPa. The very different response of each G-zone indicates variations in elastic limit strength, hardening behaviour and deformation modulus along the specimen when stressed in the strain-hardening domain as illustrated in Fig. 7.

4.3 Deformation growth due to fatigue

4.3.1 Introduction

Tensile fatigue testing was conducted while imposing constant maximum and minimum stresses, and the growth of specimen deformation as a function of stress cycles was recorded. There are thus some similarities with tensile creep testing. Fatigue deformation growth may thus include some creep deformation.

In the following, recorded deformation growth of UHPFRC specimens from the S1 series only is examined. In fact, in the S2 and S3 series, specimens showed no significant deformation growth as these specimens had already some initial deformation due to the preloading prior to the fatigue test. The deformation growth during the fatigue test was then relatively small and constant. Only in the final phase before failure, deformations increased substantially.
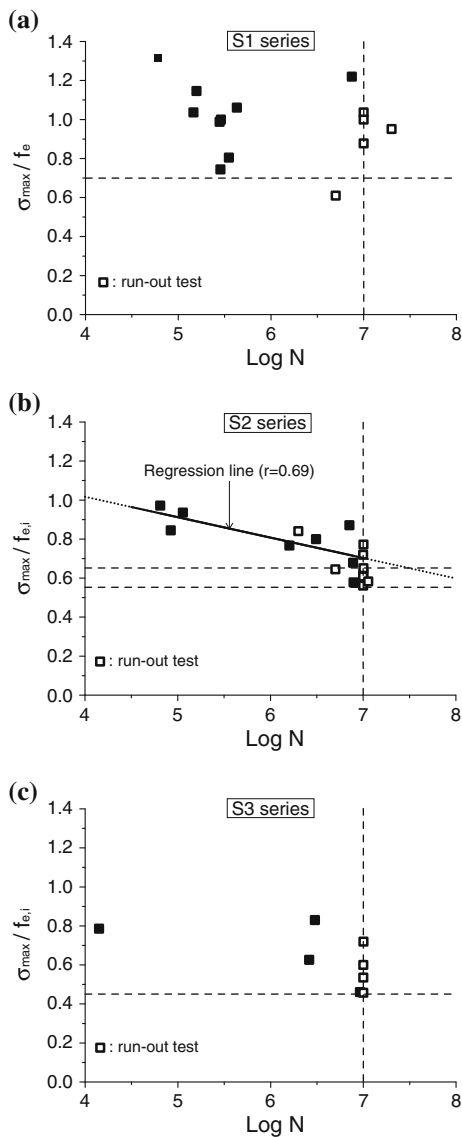
Fig. 5 S–N diagrams of **a** S1 series, **b** S2 series and **c** S3 series

4.3.2 Deformation growth from S1 series

Fatigue deformation as recorded from the S1 series may be subdivided into four distinct types of behaviour:

(1) Redistribution of localised deformation

Specimen S1-3 showed after about 9.1 million fatigue cycles a sudden increase in deformation in the G1 zone leading to a macrocrack with an opening reaching about 0.1 mm (Fig. 8b). The specimen continued then to carry fatigue stress cycles up to 20 million cycles. This observation again confirms the
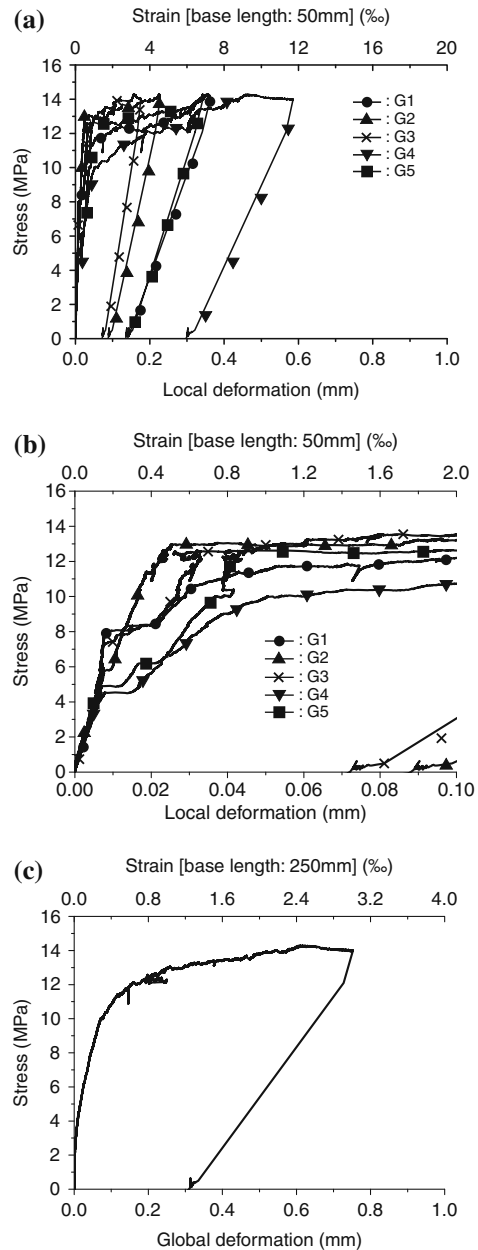
Fig. 6 Stress-deformation curves obtained from quasi-static tensile preloading preceding the S4-1 tests **a** local deformation, **b** zoom of stress-local deformation curve [0–0.1 mm], **c** global deformation

capacity of UHPFRC to redistribute localised deformation. It is interesting to note that this localised deformation could not be captured by the global deformation readings (Fig. 8a) because this localisation occurred outside the measuring domain of the LVDTs for global deformation.
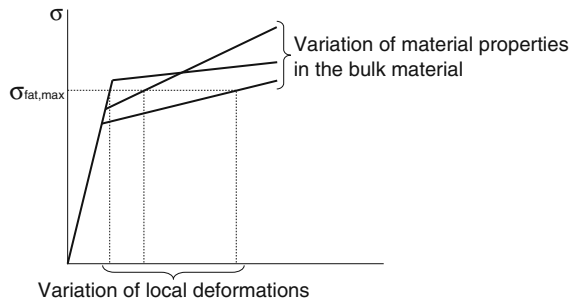
Fig. 7 Variation of local deformation of UHPFRC under constant tensile fatigue stress

After 20 million stress cycles, maximum stress was increased from 7.8 to 8.7 MPa (S1-3_ii test), and similar deformation localisation occurred in two different zones (G2 and G3 zones), while the specimen continued to carry fatigue stress (Fig. 9). Finally, the specimen failed in G2 zone at 428,072 cycles while the two other zones with deformation localisation showed decreasing deformation values towards the end of the test.

Similar deformation growth curves were recorded from other specimens. It seems that even after localisation of deformation resulting in macrocrack openings of 0.1 mm, UHPFRC has the capacity to carry on tensile fatigue cycles by redistribution of localised deformation. The mechanism of this redistribution is supposed to be based on arresting further macrocrack growth when it enters into a zone with denser and better orientated fibres.

(2) Variations in local deformation

Variations in local deformation measured with the five displacement transducers were also observed in tensile fatigue tests.

Figure 10b shows the growth of local deformations during the S1-5_ii test as a function of fatigue cycles. Deformation of the G4 zone increased very rapidly during the first 9,000 cycles, and after 9,000 cycles its growth rate became suddenly relatively low. This may be attributed to the capacity of the UHPFRC to redistribute deformation under a given imposed stress while probably developing some change in microcrack pattern. Deformation development of the G3 and G5 zones was similar during the first 9,000 cycles; then, the deformation growth rate of the G3 zone became higher, while the deformation growth rate of the G5 zone reduced significantly to almost zero. The
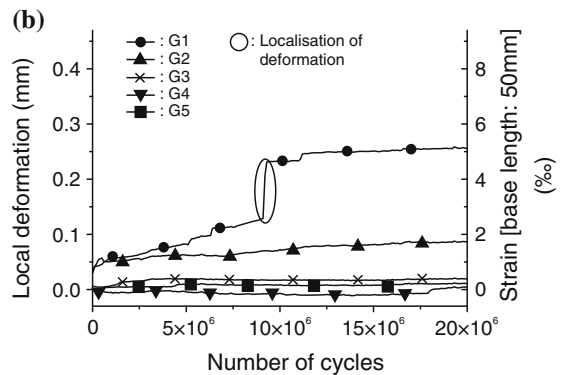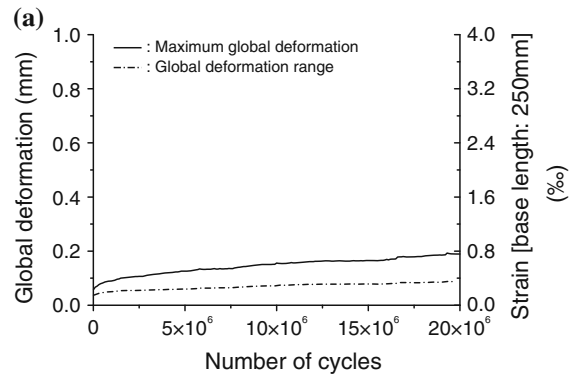

Fig. 8 Deformation growth curve of the S1-3_i test **a** global deformation and global deformation range, **b** local deformation

deformation growth rate of the G1 and G2 zones was quite constant during the fatigue test, implying that these zones were not influenced by deformation redistribution that occurred at 9,000 cycles. It can also be noted that deformation and deformation growth rate of the G1 and G3 zone were similar after 32,000 cycles until failure, and deformation of the G2 zone was gradually approaching deformation of the G5 zone.

Fatigue fracture occurred in the G4 zone. Consequently, deformation growth curve of the G4 zone was similar to the global deformation growth curve (Fig. 10a). Although deformation behaviour of each G-zone influenced global specimen behaviour, the G4 zone predominantly influenced the global deformation behaviour of this specimen. From this it may be stated that the G1 to G3 and G5 zones were intact and still had fatigue stress carrying capacity after the fatigue fracture of the specimen.

(3) Change in deformation range

The deformation range, i.e. difference between maximum and minimum deformation, became larger
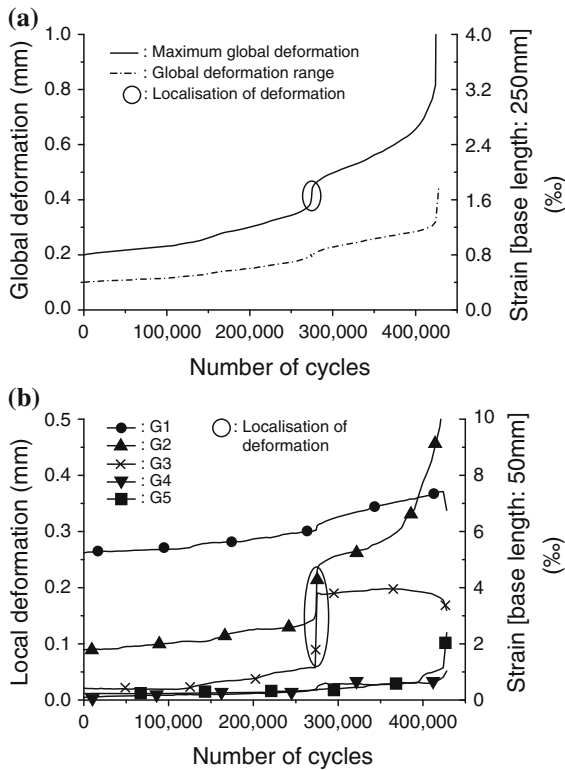
Fig. 9 Deformation growth curve of the S1-3_ii test **a** global deformation and global deformation range, **b** local deformation

Fig. 10 Deformation growth curve of the S1-5_ii test **a** global deformation and global deformation range, **b** local deformation

with increasing number of fatigue cycles. The increase in rate of the deformation range was slightly smaller than that of maximum deformation, but the trends of both rates were similar. As stress cycles increased, maximum deformation also increased while minimum deformation remained almost constant, as shown in Figs. 8a, 9a and 10a where the dashed line represents the global deformation range.

(4) Deformation growth and evolution of deformation modulus

Figure 11 shows the maximum global deformation plotted against the modulus of deformation E calculated as follows:

$$E = \frac{\sigma_{\max} - \sigma_{\min}}{\varepsilon_{\max,i} - \varepsilon_{\min,i}} \quad (2)$$

where $\sigma_{\max}$ and $\sigma_{\min}$ are the applied maximum and minimum fatigue stress (being constant); $\varepsilon_{\max,i}$ and $\varepsilon_{\min,i}$ are maximum and minimum global strain at cycle i. These curves were constructed for all specimens of the S1 series.
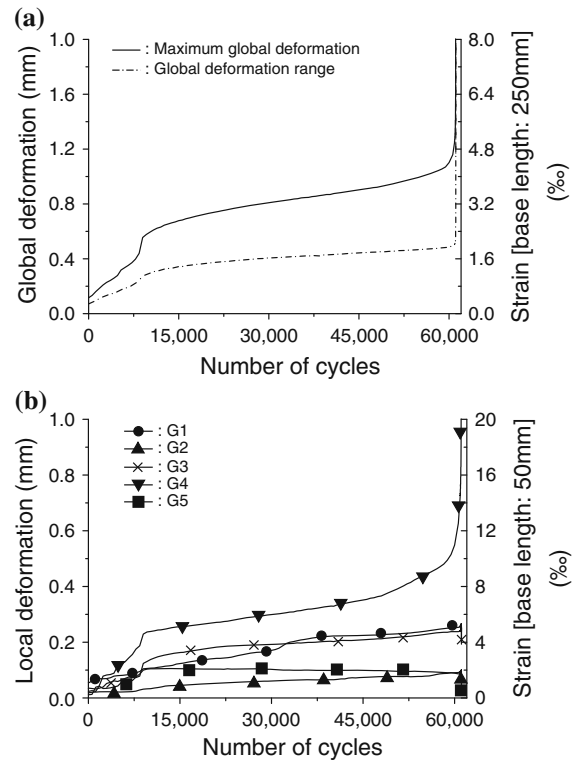
All curves show a similar trend despite the differences in applied stress level. A strong decrease of deformation modulus of UHPFRC is observed when the material enters into the domain corresponding to the strain-hardening domain observed in the quasi-static tensile test ("the equivalent strain-hardening domain" hereafter). Deformation modulus of UHPFRC decreases from about 38.9 to 9.7 GPa when the material global strain grows from 0.32 to 1.66 ‰ corresponding respectively to the elastic limit and ultimate strength of UHPFRC determined from three quasi-static tensile tests. Thus, the stress carrying capacity of UHPFRC under tensile fatigue significantly decreases when the material deformation is within the equivalent strain-hardening domain. Habel [15] reported similar findings from cyclic tensile tests on a different UHPFRC mix (CEMTEC$_{\text{multiscale}}$©).

Decrease in the deformation modulus within the strain-hardening domain may be caused by progressive matrix cracking and fibre pull-out. In the softening domain, the decrease of deformation modulus
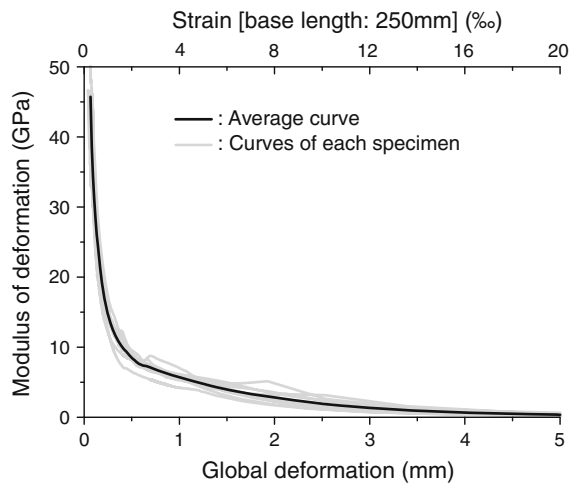
Fig. 11 Relation between maximum global deformation and modulus of deformation

Fig. 12 Fracture surface showing matrix spalling and pulverization

became lower because of deformation localisation occurring in the macrocrack; further matrix cracking stopped and fibre pull-out occurred only in the localised macrocrack.

4.4 Uniaxial tensile tests

All the quasi-static and fatigue tests in this paper were conducted in the mode of uniaxial tension. Due to the possibility of asymmetric crack formation causing the specimens to bend, it was considered that uniaxial tensile force wasn't properly imposed on the specimens.

In order to investigate if the tests were done in uniaxial tension, the possibility of asymmetric crack formation was monitored by setting up displacement transducers on both surfaces of several specimens (five displacement transducers on each surface) during the S2 and S3 series. Deflection of the specimens wasn't explicit in measurements of the displacement transducers. Therefore, applied tensile force was regarded as uniaxial.

4.5 Fracture surface

4.5.1 Introduction

Fracture surfaces may provide important information to understand failure of materials. Fractography,

aiming to analyse the characteristics of a fracture surface to indicate fracture mechanisms [16], has been used for failure analysis of metals for several decades. Since UHPFRC shows features of mechanical behaviour of metals, UHPFRC fatigue fracture surfaces were analysed by fractography to understand the fracture mechanisms of UHPFRC under tensile fatigue. Visual observation of fracture surfaces revealed three specific features as discussed in the following.

4.5.2 Matrix spalling and pulverisation

Figure 12 shows the fracture surface of a specimen that sustained more than 10 million fatigue cycles. Spalling of small matrix particles and pulverised matrix can be identified. It is speculated that pulverized matrix also contains unhydrated cement and silica fume. Spalling might have occurred when fibres were partially or fully pulled out of the matrix in a direction other than the fibre axis [17], as shown on Fig. 11a. This mechanism is called snubbing [18], and bent fibres also observed on fracture surfaces are just a consequence of snubbing (Fig. 13b).

Pulverisation of the matrix may be due to abrasion of spalling particles while the irregular faces of the rough fracture surface were subjected to fretting and grinding under fatigue cycles. As the fracture surfaces must be in contact for fretting, this mechanism can be referred to as roughness-induced closure which is one of the fatigue crack closure mechanisms in metals [19].

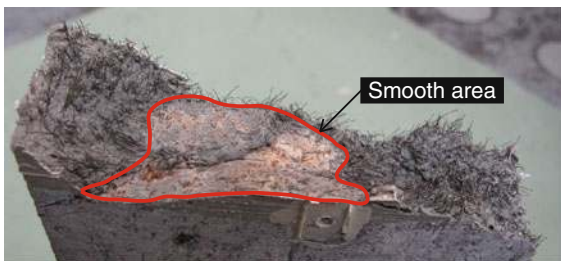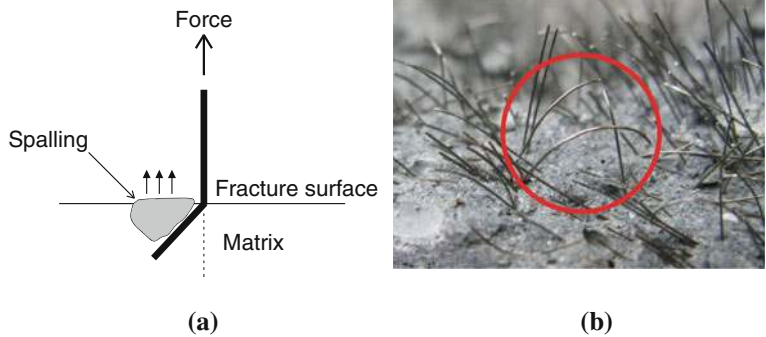**Fig. 13 a** Snubbing of fibre (after [18]), and **b** Bent fibres due to snubbing

(a) **(b)**

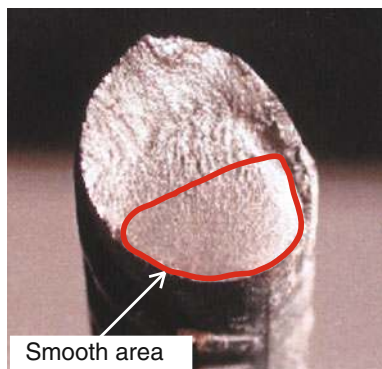**Fig. 14** Smooth area of fatigue fracture surface of UHPFRC

Fig. 15 Fatigue fracture surface of a steel rebar [20]

4.5.3 Smooth fracture surface area

Figure 14 shows a distinct area where the surface is smooth and shows only few fibres when compared to the rest of the fatigue fracture surface. This smooth area coincides with the location of fatigue fracture initiation. Similar smooth area is also observed on fatigue fracture surface of steel (Fig. 15).

Two processes may explain the formation of a smooth fatigue fracture surface area:

– Due to the UHPFRC fabrication process, there is some variation in fibre distribution in the material volume, and consequently, local zones with smaller fibre content may exist [13]. Such zones have a lower stress carrying capacity and precocious microcracking is rather likely to occur leading to a significant fretting and grinding of the microcrack surfaces polishing them.

– A second process may be due to tribocorrosion fracture of fibres: fibres transfer tensile stress across micro- and macrocracks through the interface with the matrix (fibre bridging) (Fig. 16). Under fatigue cycles, fibre pull-out and slip-back movement occurs after debonding of the fibres from the matrix (Fig. 17), wearing away both the fibres and the matrix [21]. In the present study, the fibres are originally coated with a thin brass layer which is first removed by abrasion with the matrix. The bare steel surface of the fibres bridging the micro- and macrocrack is now exposed to the atmosphere. However, average relative humidity is about 40 % in the testing hall and corrosion of
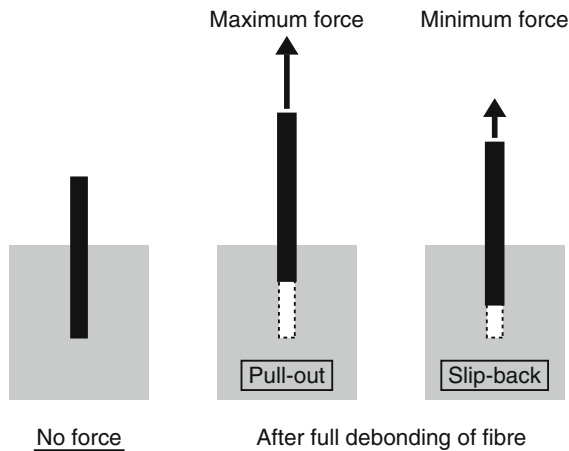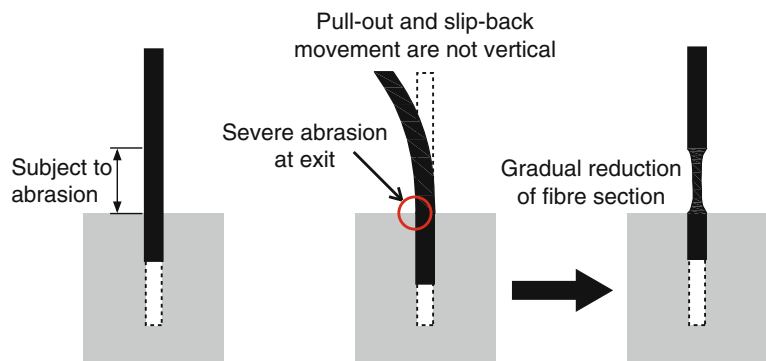
Fig. 16 Fibre bridging at cracked section
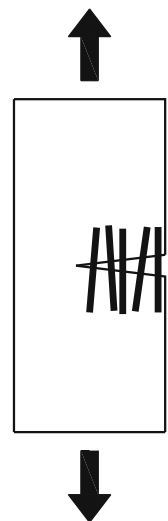
Fig. 17 Fibre pull-out and slip-back movement

the bare steel is unlikely to occur because the corrosion rate of iron increases significantly at 60 % relative humidity [22]. More humidity or lower corrosion potential would thus be necessary for corrosion of the bare steel. As all water is consumed in the process of cement hydration in UHPFRC, supply of more humidity seems to be improbable. Lowering of corrosion potential can also be caused by wear of fibres with matrix, which is known as tribocorrosion phenomena which leads to corrosion of bare steel even in atmospheres with low humidity [23]. Corroding fibres bridging the fracture surface gradually lose their volume and are eventually fractured rather than pulled out of the matrix (Fig. 18).

It may be stated that fatigue fracture mechanism of UHPFRC and steel seems to be similar. A macrocrack is initiated from the weakest location in the element and propagates under fatigue stress cycles. Gradually, the element loses its stress carrying capacity (resulting

in a decrease in modulus of deformation). Finally, when the applied maximum fatigue stress reaches the ultimate resistance of the uncracked remaining cross section, the specimen fails. Fatigue crack propagation is identified by the smooth surface while final fracture leads to rather rough surface of UHPFRC.

Although fatigue fracture mechanisms of UHPFRC and steel show some similarities, fatigue crack propagation behaviour of UHPFRC and steel is dissimilar because of the difference in material structure. At meso-level, fatigue crack propagation in UHPFRC occurs when fibres are pulled out or fractured, and its behaviour might depend on fibre distribution. On the contrary, material structure of steel in meso-level is homogeneous and fatigue crack propagation occurs due to microplastic deformation [24].

4.5.4 Rust-coloured powdery products

It was systematically observed that rust-coloured powdery products covered a part of the fracture surface, nearly matching the smooth surface area. Rust colour in small area around fibres was thicker than in other areas, implying that rust-coloured powdery products were provided by corrosion products from the fibres. Also, the rust-coloured powdery products were supposed to be mixes of pulverised matrix and corrosion products. In order to confirm this supposition, energy dispersive X-ray spectroscopy (EDS) was used to analyse these powdery products, and the fracture surface of S4-2 test specimen covered with the rust-coloured powdery products was examined using a scanning electron microscope (SEM).

Figure 19 shows the material composition of powdery products taken form the fracture surface analysed
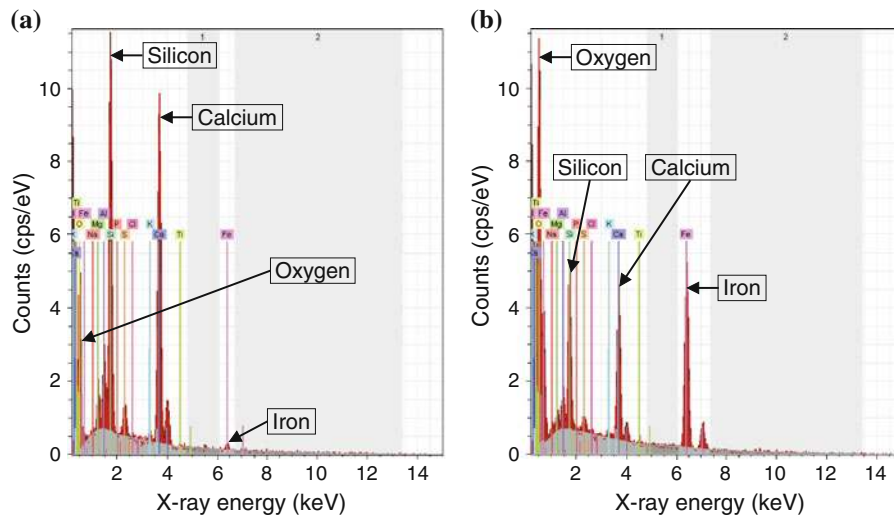
Fig. 18 Abrasion of fibre with matrix

Fig. 19 Material composition of products from the fracture surface of the S4-2 tests specimen **a** normally coloured area, **b** rust-coloured area
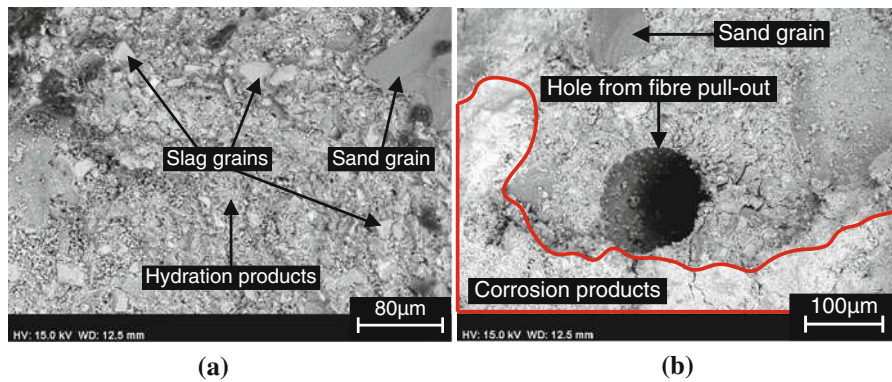

Fig. 20 SEM images of fatigue fracture surface (S4-2 tests specimen) **a** normally-coloured and **b** rust-coloured areas
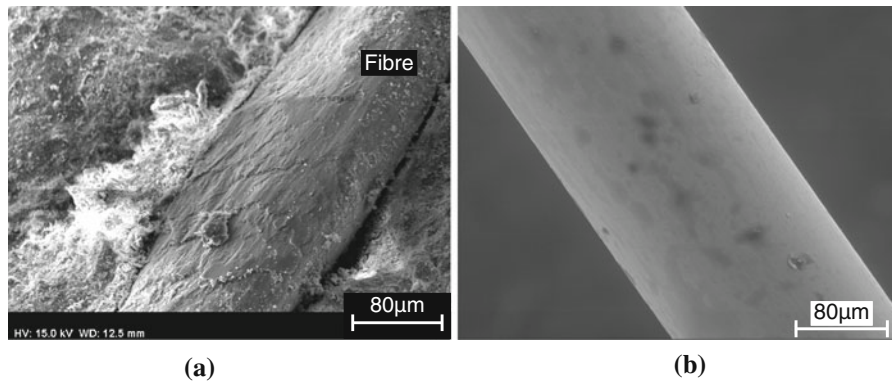

Fig. 21 SEM images of steel fibres: **a** steel fibre from the rust-coloured area of fracture surface, **b** steel fibre in its original condition

by EDS. Major components of normally coloured products were silicon and calcium, which are main matrix components while rust-coloured products had significant amounts of iron and oxygen, i.e. iron oxide, confirming the existence of corrosion products. Moreover, SEM analysis of fracture surface revealed the existence of significant amounts of corrosion products in rust-coloured area.

Figure 20 shows SEM images of both normally coloured and rust-coloured areas of fatigue fracture surface of the S4-2 test specimen. In the normally coloured area, components of matrix such as hydration products, sand and slag grains were identified. In the rust-coloured area, whitish parts indicate corrosion products and a hole seems to be created by fibre pull-out.

Figure 21a shows a steel fibre in the rust-coloured area. Rough fibre surface is clearly recognised. This is in contrast with the surface of a steel fibre (of same type) in its original condition (Fig. 21b) with a flat and smooth surface. Figure 21a also suggests that the fibre surface (from the rust-coloured area) was roughened by abrasion and fretting with the surrounding matrix.

5 Conclusions

The following conclusions can be drawn regarding the tensile fatigue behaviour of UHPFRC as obtained from uniaxial constant amplitude tensile fatigue tests:

1. The elastic limit strength seems to be a significant property to describe the fatigue strength of UHPFRC. A method is proposed to determine the elastic limit strength.
2. UHPFRC shows a fatigue endurance limit with respect to 10 million cycles above which fatigue stress induces significant damage leading to rather short fatigue lives. An endurance limit was obtained in all three domains of UHPFRC tensile behaviour and at a stress levels of (1) $S = 0.7$ in the elastic domain, (2) $S = 0.6$ in the strain hardening domain and (3) $S = 0.45$ in the strain softening domain, for S being the ratio between the maximum fatigue stress and the elastic limit strength of UHPFRC.
3. UHPFRC specimens subjected to a given tensile stress show rather large differences in local deformations. This is due to variations in material

properties, in particular elastic limit strength and strain hardening behaviour. These variations in local deformation confer significant stress and deformation redistribution capacity to the UHPFRC bulk material enhancing thus the fatigue behaviour.
4. The fatigue fracture surface of UHPFRC shows features of fatigue fracture surfaces of steel. Fatigue crack propagation is identified by a smooth surface while final fracture leads to rather rough surface.
5. UHPFRC fatigue fracture surface shows clear signs of matrix spalling and pulverisation which is the result of snubbing, fibre pull-out—slip-back movements as well as abrasion of fibres with the matrix, due to fretting and grinding under fatigue cycles. Smooth areas also show rust-coloured powdery products which are due to tribocorrosion as depicted by spectroscopy and SEM analyses.

References

1. Denarié E, Brühwiler E (2006) Structural rehabilitations with ultra high performance fibre reinforced concretes. Int J Restor Build Monum 12(5 and 6): 453–465
2. Brühwiler E, Denarié E (2008) Rehabilitation of concrete structures using ultra-high performance fibre reinforced concrete. In: Fehling E, Schmidt M, Stürwald S (eds) Proceedings of UHPC-2008: the second international symposium on ultra high performance concrete, Kassel, pp 895–902
3. Brühwiler E (2009) Rehabilitation of bridges using ultra-high performance fiber reinforced concrete. In: Proceedings of 5th New York City Bridge Conference, New York
4. Brühwiler E (2010) Ultra-high performance fiber reinforced concrete improves concrete structures. Structural concrete in Switzerland, Swiss national group of the international federation for structural concrete, pp 145–149
5. Lappa ES, René Braam C, Walraven JC, (2006) Flexural fatigue of high and ultra high strength fiber reinforced concrete. In: Fischer G, Li VC (eds) Proceedings of international RILEM workshop on high performance fiber reinforced cementitious composites in structural applications, pp 509–518
6. Behloul M, Chanvillard G, Pimienta P, (2005) Fatigue flexural behavior of pre-cracked specimens of special UHPFRC. In: Proceedings of seventh international symposium on the utilization of high-strength/high-performance concrete, ACI Symposium Publication 228, Washington, DC, pp 1253–1268
7. Farhat FA, Nicolaides D, Kanellopoulos A, Karihaloo BL (2005) High performance fibre-reinforced cementitious composite (CARDIFRC)—performance and application to retrofitting. Eng Fract Mech 74(1–2):151–167

8. Parant E, Rossi P, Boulay C (2007) Fatigue behaviour of a multi-scale composite. Cem Concr Res 37:264–269

9. Fitik B, Niedermeier R, Zilch K (2009) Fatigue behaviour of ultra high performance concrete under cyclic stress reversal loading. In: Denton S, Clark G (eds) Proceedings of the 11th annual international fib symposium—Concrete: 21st Century Superhero, London

10. Fitik B, Niedermeier R, Zilch K (2010) Fatigue behaviour of ultra-high performance concrete under cyclic stress reversal loading. In: Proceedings of third international fib congress incorporating the PCI annual convention and bridge conference, Washington, DC, pp 5393–5402

11. Cornelissen HAW (1984) Fatigue failure of concrete in tension. Heron 29(4):1–68

12. Sadananda K, Vasudevan AK, Phan N (2007) Analysis of endurance limits under very high cycle fatigue using a unified damage approach. Int J Fatigue 29:2060–2071

13. Wuest J (2007) Comportement structural des bétons de fibres ultra performants en traction dans des éléments composé. Doctoral thesis, Ecole Polytechnique Fédérale de Lausanne

14. Oesterlee C, Sadouki H, Brühwiler E, (2008) Structural analysis of a composite bridge girder combining UHPFRC and reinforced concrete. In: Fehling E, Schmidt M, Stürwald S (eds) Proceedings of UHPC-2008: the second international symposium on ultra high performance concrete, Kassel, 05–07 March 2008, pp 647–654

15. Habel K (2004) Structural behaviour of elements combining ultra-high performance reinforced concretes (UHPFRC) and reinforced concrete. Doctoral thesis, Ecole Polytechnique Fédérale de Lausanne

16. ASM Handbook Committee (1987) ASM handbook Volume 12: Fractography, ASM International, Materials Park

17. Brandt AM (1985) On the optimal direction of short metal fibres in brittle matrix composites. J Mater Sci 20(11):3831–3841

18. Li VC, Backer S (1990) Effect of inclining angle, bundling and surface treatment on synthetic fibre pull-out from a cement matrix. Composites 21(2):132–140

19. Anderson TL (2005) Fracture mechanics: fundamentals and applications, 3rd edn, CRC Press, Boca Raton

20. Johansson U (2004) Fatigue tests and analysis of reinforced concrete bridge deck models. Licentiate thesis, Royal Institute of Technology, Sweden

21. Zhang J, Stang H, Li VC (2001) Crack bridging model for fibre reinforced concrete under fatigue tension. Int J Fatigue 23(8):655–670

22. ASM Handbook Committee (1987) ASM Handbook Volume 13: Corrosion, ASM International, Materials Park

23. Landolt D (2007) Corrosion and surface chemistry of metals, EPFL Press, Lausanne

24. Schijve J (2009) Fatigue of structures and materials, Springer, Berlin